ANS M&C 2021 - The International Conference on Mathematics and Computational Methods Applied to Nuclear Science and Engineering · Raleigh, North Carolina · October 3–7, 2021

DISCONTINUOUS GALERKIN VARIABLE EDDINGTON FACTOR METHODS*

Samuel Olivier[1]†, Terry S. Haut[2], and Ben C. Yee[2]

[1]University of California, Berkeley
Berkeley, CA

[2]Lawrence Livermore National Laboratory
Livermore, CA

solivier@berkeley.edu

ABSTRACT

We derive an arbitrary-order Discontinuous Galerkin Variable Eddington Factor method that is effective on a linearized thermal radiative transfer problem in both transport outer iterations and inner preconditioned BiCGStab iterations while supporting the use of a negative flux fixup inside the iteration. The inner iterations are shown to be uniform in the mesh size, polynomial order, and penalty parameter.

KEYWORDS: VEF; DG; high-order FEM

1. INTRODUCTION

The Variable Eddington Factor (VEF) method [1], also known as Quasidiffusion (QD) [2], is a rapidly-converging nonlinear scheme for solving the radiation transport equation. In contrast to traditional acceleration methods, such as Diffusion Synthetic Acceleration (DSA), VEF methods enable significant algorithmic flexibility including the use of so-called "independent" discretizations [3–5] and negative flux fixups [6] while still retaining the thick diffusion limit.

In this work, we leverage VEF's discretization flexibility to design independent VEF methods that both converge rapidly *and* can be efficiently solved using preconditioned iterative solvers. In [7], it is shown that Discontinuous Galerkin (DG) discretizations of elliptic equations can be effectively solved independent of the mesh size, finite element polynomial order, and penalty parameter through the use of a subspace correction preconditioner. By carefully following [8], we derive a family of DG VEF methods that are effectively preconditioned by this subspace correction method. We show that an interior penalty-like VEF method has arbitrary order accuracy, maintains the thick diffusion limit, and can be efficiently solved independent of the mesh size, polynomial order, and

*Reviewed for release under LLNL-CONF-820504.

†SO is supported by the Department of Energy Computational Science Graduate Fellowship under grant number DE-SC0019323.

penalty parameter. This method is shown to be effective both in outer transport iterations and inner linear solver iterations on the linearized crooked pipe problem, a difficult proxy problem from thermal radiative transfer, even when a negative flux fixup is used inside the iteration.

2. THE INDEPENDENT VEF METHOD

Here we describe the VEF method for a planar geometry, mono-energetic, fixed-source transport problem with isotropic scattering discretized in angle with the Discrete Ordinates (S_N) angular model. The coupled transport-VEF system is:

$$\boldsymbol{\Omega} \cdot \nabla \psi_d + \sigma_t \psi_d = \frac{\sigma_s}{4\pi} \varphi + q_d \,, \tag{1a}$$

$$\nabla \cdot (\mathbf{E}\varphi) + \sigma_t \boldsymbol{J} = \boldsymbol{Q}_1 \,, \tag{1b}$$

$$\nabla \cdot \boldsymbol{J} + \sigma_a \varphi = Q_0 \,, \tag{1c}$$

where ψ_d and q_d are the angular flux and fixed-source in direction $\boldsymbol{\Omega}_d$, Q_0 and $\boldsymbol{Q}_1$ the zeroth and first angular moments of the fixed-source, φ the VEF scalar flux, $\boldsymbol{J}$ the VEF current, and

$$\mathbf{E}(\mathbf{x}) = \frac{\sum_d w_d \, \boldsymbol{\Omega}_d \otimes \boldsymbol{\Omega}_d \, \psi_d(\mathbf{x})}{\sum_d w_d \psi_d(\mathbf{x})} \tag{2}$$

the Eddington tensor. Note that when an independent discretization is used for the VEF equations φ and $\boldsymbol{J}$ will not be equivalent to the zeroth and first angular moments of the discrete angular flux. To notationally separate the two scalar flux solutions, we define

$$\phi(\mathbf{x}) = \sum_d w_d \psi_d(\mathbf{x}) \,, \tag{3}$$

as the zeroth angular moment of the angular flux and stress again that in general φ and ϕ are not equivalent. Due to the Eddington tensor, the transport equation is nonlinearly coupled to the VEF equations. However, by construction, the Eddington tensor is a weak function of the angular flux meaning even fixed point iteration converges quickly. Fixed-point iteration refers to alternating between solving the transport equation with lagged scattering source and solving the VEF equations with lagged VEF data until the VEF scalar flux converges.

In this work, we assume that the transport equation is discretized with a high-order DG discretization (e.g. [9]). In such case, the angular flux in direction $\boldsymbol{\Omega}_d$ lives in a discrete subspace of

$$Y = \{u \in L^2(\mathcal{D}) : u|_K \in H^1(K) \quad \forall K \in \mathcal{T}\} \,, \tag{4}$$

the space of piecewise discontinuous functions that are locally smooth on each element K in the mesh $\mathcal{T}$. Through the standard finite element interpolation procedure, the Eddington tensor can then be evaluated at any location in the mesh using Eq. 2. Note that it is important to interpolate the numerator and denominator of the Eddington tensor *independently*. Given $\psi_d \in Y$ and $\phi > 0$, we have that each component of the Eddington tensor is also in Y.

It is helpful to define the "broken" gradient, denoted by ∇_h, as applying the gradient locally on each element. That is,

$$(\nabla_h u)|_K = \nabla(u|_K) \,, \quad \forall K \in \mathcal{T} \,. \tag{5}$$

This is important since, for $u \in Y$, ∇u is undefined due to the piecewise discontinuous nature of the space Y while $\nabla_h u$ is well-defined since u is locally differentiable on each element. Defining $\mathbf{P} = \sum_d w_d \, \mathbf{\Omega}_d \otimes \mathbf{\Omega}_d \, \psi_d$ and using the quotient rule,

$$\nabla_h \cdot \mathbf{E} = \frac{(\nabla_h \cdot \mathbf{P}) \, \phi - \mathbf{P} \cdot \nabla_h \phi}{\phi^2} \tag{6}$$

is well-defined since $\nabla_h \psi_d$ is. To support generality, we assume that the finite element space for the VEF scalar flux and the finite element space for the angular fluxes are different. The scattering source is then constructed using a mixed space mass matrix that has test functions in the space for ψ_d and trial functions in the space for φ.

Defining transport-consistent boundary conditions completes the description of the independent VEF method. Here, we assume inflow boundary conditions of the form:

$$\psi_d(\mathbf{x}) = \bar{\psi}_d(\mathbf{x}) \, , \quad \mathbf{x} \in \partial\mathcal{D} \text{ and } \mathbf{\Omega}_d \cdot \hat{n} < 0 \, , \tag{7}$$

where vacuum conditions are the special case that $\bar{\psi}_d = 0$. The Miften-Larsen VEF boundary conditions are:

$$\bar{J}_{\text{in}} = \frac{1}{2} \left(\boldsymbol{J} \cdot \hat{n} - E_b \varphi \right) \, , \quad \mathbf{x} \in \partial\mathcal{D} \, , \tag{8}$$

where

$$\bar{J}_{\text{in}} = \sum_{\mathbf{\Omega}_d \cdot \hat{n} < 0} w_d \, \mathbf{\Omega}_d \cdot \hat{n} \, \bar{\psi}_d \, , \tag{9a}$$

$$E_b = \frac{\sum_d w_d \, |\mathbf{\Omega}_d \cdot \hat{n}| \, \psi_d}{\sum_d w_d \psi_d} \, . \tag{9b}$$

Again, since ψ_d is provided as a grid function, the Eddington boundary factor, E_b, can be evaluated anywhere on the boundary of the mesh.

3. DERIVATION OF DG VEF

In this section, we adapt the derivation of the DG methods designed for the Poisson equation provided in [8] to the VEF equations. There, the authors derive a family of DG methods for:

$$\boldsymbol{q} = \nabla u \, , \tag{10a}$$

$$-\nabla \cdot \boldsymbol{q} = f \, , \tag{10b}$$

with Dirichlet boundary conditions. The present goal is to adapt their derivation to the VEF equations:

$$\nabla \cdot (\mathbf{E} \varphi) + \sigma_t \boldsymbol{J} = \boldsymbol{Q}_1 \, , \tag{11a}$$

$$\nabla \cdot \boldsymbol{J} + \sigma_a \varphi = Q_0 \, , \tag{11b}$$

with the Robin boundary conditions given in Eq. 8. We will see significant differences in the final equation since the Eddington tensor is inside the divergence. Additionally, the presence of a right hand side in the first moment equation as well as non-unit coefficients introduce complications not discussed in [8].

We seek the scalar flux in the finite element space

$$Y_p = \{u \in L^2(\mathcal{D}) : u|_K \in \mathbb{Q}_p(K) \quad \forall K \in \mathcal{T}\} \tag{12}$$

and the current in the space

$$W_p = \{\boldsymbol{v} \in \left[L^2(\mathcal{D})\right]^{\dim} : \boldsymbol{v}|_K \in [\mathbb{Q}_p(K)]^{\dim} \quad \forall K \in \mathcal{T}\}\,, \tag{13}$$

where $\mathbb{Q}_p$ is the space of polynomials of degree at most p in *all* $\dim$ spatial variables. The weak form is then: find $(\varphi, \boldsymbol{J}) \in Y_p \times W_p$ such that for all $K \in \mathcal{T}$

$$\int_{\partial K} \boldsymbol{v} \cdot \widehat{\mathbf{E}\varphi}\hat{n}\,\mathrm{d}s - \int_K \nabla \boldsymbol{v} : \mathbf{E}\varphi\,\mathrm{d}\mathbf{x} + \int_K \sigma_t\, \boldsymbol{v} \cdot \boldsymbol{J}\,\mathrm{d}\mathbf{x} = \int_K \boldsymbol{v} \cdot \boldsymbol{Q}_1\,\mathrm{d}\mathbf{x}\,, \quad \forall \boldsymbol{v} \in [\mathbb{Q}_p(K)]^{\dim}\,, \tag{14a}$$

$$\int_{\partial K} u\,\widehat{\boldsymbol{J}} \cdot \hat{n}\,\mathrm{d}s - \int_K \nabla u \cdot \boldsymbol{J}\,\mathrm{d}\mathbf{x} + \int_K \sigma_a\, u\varphi\,\mathrm{d}\mathbf{x} = \int_K u\, Q_0\,\mathrm{d}\mathbf{x}\,, \quad \forall u \in \mathbb{Q}_p(K)\,, \tag{14b}$$

where the *numerical fluxes* $\widehat{\mathbf{E}\varphi}$ and $\widehat{\boldsymbol{J}}$ are approximations of $\mathbf{E}\varphi$ and $\boldsymbol{J}$ on the boundary of each element K. We group the product $\mathbf{E}\varphi$ as a numerical flux to mimic the integration by parts of a tensor times a vector.

Summing the zeroth moment over all elements:

$$\int_\Gamma [\![u]\!] \left\{\!\!\left\{ \widehat{\boldsymbol{J}} \cdot \hat{n} \right\}\!\!\right\} \mathrm{d}s + \int_{\Gamma_0} \{\!\{u\}\!\} \left[\!\!\left[\widehat{\boldsymbol{J}} \cdot \hat{n} \right]\!\!\right] \mathrm{d}s - \int \nabla_h u \cdot \boldsymbol{J}\,\mathrm{d}\mathbf{x} + \int \sigma_a\, u\varphi\,\mathrm{d}\mathbf{x} = \int u\, Q_0\,\mathrm{d}\mathbf{x}\,, \tag{15}$$

where Γ is the set of all unique faces in the mesh and $\Gamma_0 = \Gamma \setminus \partial\mathcal{D}$ the set of unique interior faces in the mesh. Additionally, define $\Gamma_b = \Gamma \cap \partial\mathcal{D}$ as the set of faces on the mesh boundary. On an interior face $\mathcal{F} \in \Gamma_0$ between elements K_e and $K_{e'}$ with normal pointing from K_e to $K_{e'}$, the jump, $[\![\cdot]\!]$, and average, $\{\!\{\cdot\}\!\}$, for scalar-valued arguments are defined as

$$[\![u]\!] = u_e - u_{e'}\,, \quad \{\!\{u\}\!\} = \frac{1}{2}(u_e + u_{e'})\,, \quad \text{on } \mathcal{F} \in \Gamma_0 \tag{16}$$

where $u_i = u|_{\partial K_i}$. For vector-valued functions:

$$[\![\boldsymbol{v}]\!] = \boldsymbol{v}_e - \boldsymbol{v}_{e'}\,, \quad \{\!\{\boldsymbol{v}\}\!\} = \frac{1}{2}(\boldsymbol{v}_e + \boldsymbol{v}_{e'})\,, \quad \text{on } \mathcal{F} \in \Gamma_0\,. \tag{17}$$

Note that these definitions deviate from those in [8] which include the normal in the definition of the jump. Our notation elects to explicitly denote the normal vector in the *arguments* of all jump and average terms which avoids the complication of the jump and average of a symmetric tensor. On the boundary of the mesh,

$$[\![u]\!] = u\,, \quad \{\!\{\boldsymbol{v}\}\!\} = \boldsymbol{v}\,, \quad \text{on } \mathcal{F} \in \Gamma_b\,. \tag{18}$$

The average of a scalar and jump of a vector on a boundary face are left undefined. Instead, we are careful to denote integration over Γ and Γ_0 so that these quantities are not needed. Above we utilized the "jumps and averages identity":

$$[\![uv]\!] = [\![u]\!]\,\{\!\{v\}\!\} + \{\!\{u\}\!\}\,[\![v]\!] \tag{19}$$

to write $\left[\!\!\left[u\,\widehat{\boldsymbol{J}} \cdot \hat{n} \right]\!\!\right]$ as two terms.

Now the goal is to determine a functional form for $\boldsymbol{J}$. Using the identity

$$\int_K \nabla \boldsymbol{v} : \mathbf{E}\varphi \,\mathrm{d}\mathbf{x} = \int_{\partial K} \boldsymbol{v} \cdot \mathbf{E}\varphi \hat{n} \,\mathrm{d}s - \int_K \boldsymbol{v} \cdot \nabla \cdot (\mathbf{E}\varphi) \,\mathrm{d}\mathbf{x} \tag{20}$$

the first moment's weak form on each element becomes:

$$\int_{\partial K} \boldsymbol{v} \cdot \left(\widehat{\mathbf{E}\varphi} \hat{n} - \mathbf{E}\varphi \hat{n} \right) \mathrm{d}s + \int_K \boldsymbol{v} \cdot \nabla \cdot (\mathbf{E}\varphi) \,\mathrm{d}\mathbf{x} + \int_K \sigma_t \, \boldsymbol{v} \cdot \boldsymbol{J} \,\mathrm{d}\mathbf{x} = \int_K \boldsymbol{v} \cdot \boldsymbol{Q}_1 \,\mathrm{d}\mathbf{x}\,, \quad \forall \boldsymbol{v} \in [\mathbb{Q}_p(K)]^{\dim}\,. \tag{21}$$

Summing over all elements and using the jumps and averages identity, we arrive at the so-called weak-strong form:

$$\begin{aligned} \int_\Gamma \{\!\{ \boldsymbol{v} \}\!\} \cdot \left[\!\!\left[\widehat{\mathbf{E}\varphi} \hat{n} - \mathbf{E}\varphi \hat{n} \right]\!\!\right] \mathrm{d}s + \int_{\Gamma_0} [\![\boldsymbol{v}]\!] \cdot \left\{\!\!\left\{ \widehat{\mathbf{E}\varphi} \hat{n} - \mathbf{E}\varphi \hat{n} \right\}\!\!\right\} \mathrm{d}s \\ + \int \boldsymbol{v} \cdot \nabla_h \cdot (\mathbf{E}\varphi) \,\mathrm{d}\mathbf{x} + \int \sigma_t \, \boldsymbol{v} \cdot \boldsymbol{J} \,\mathrm{d}\mathbf{x} = \int \boldsymbol{v} \cdot \boldsymbol{Q}_1 \,\mathrm{d}\mathbf{x}\,, \quad \forall \boldsymbol{v} \in W_p\,, \end{aligned} \tag{22}$$

where $\nabla_h \cdot (\mathbf{E}\varphi)$ is evaluated using the product rule as $\mathbf{E}\nabla_h \varphi + (\nabla_h \cdot \mathbf{E})\,\varphi$ with $\nabla_h \cdot \mathbf{E}$ given in Eq. 6. We now wish to write all terms as volumetric integrals so that we can determine an equation for $\boldsymbol{J}$. To that end, define lifting operators $\boldsymbol{r}(\boldsymbol{\tau}) \in W_p$ and $\boldsymbol{\ell}(\boldsymbol{\chi}) \in W_p$ such that

$$\int \sigma_t \, \boldsymbol{v} \cdot \boldsymbol{r}(\boldsymbol{\tau}) \,\mathrm{d}\mathbf{x} = -\int_\Gamma \{\!\{ \boldsymbol{v} \}\!\} \cdot \boldsymbol{\tau} \,\mathrm{d}s\,, \quad \forall \boldsymbol{v} \in W_p\,, \tag{23a}$$

$$\int \sigma_t \, \boldsymbol{v} \cdot \boldsymbol{\ell}(\boldsymbol{\chi}) \,\mathrm{d}\mathbf{x} = -\int_{\Gamma_0} [\![\boldsymbol{v}]\!] \cdot \boldsymbol{\chi} \,\mathrm{d}s\,, \quad \forall \boldsymbol{v} \in W_p\,. \tag{23b}$$

Setting $\boldsymbol{\tau} = \left[\!\!\left[\widehat{\mathbf{E}\varphi} \hat{n} - \mathbf{E}\varphi \hat{n} \right]\!\!\right]$ and $\boldsymbol{\chi} = \left\{\!\!\left\{ \widehat{\mathbf{E}\varphi} \hat{n} - \mathbf{E}\varphi \hat{n} \right\}\!\!\right\}$, Eq. 22 becomes:

$$\int \sigma_t \, \boldsymbol{v} \cdot \boldsymbol{J} \,\mathrm{d}\mathbf{x} = \int \sigma_t \, \boldsymbol{v} \cdot \left[\frac{1}{\sigma_t} \left(\boldsymbol{Q}_1 - \nabla_h \cdot (\mathbf{E}\varphi) \right) + \boldsymbol{r}\left(\left[\!\!\left[\widehat{\mathbf{E}\varphi} \hat{n} - \mathbf{E}\varphi \hat{n} \right]\!\!\right] \right) + \boldsymbol{\ell}\left(\left\{\!\!\left\{ \widehat{\mathbf{E}\varphi} \hat{n} - \mathbf{E}\varphi \hat{n} \right\}\!\!\right\} \right) \right] \mathrm{d}\mathbf{x}\,. \tag{24}$$

Subtracting the left hand side and setting the integrand to zero implies that

$$\boldsymbol{J} = \frac{1}{\sigma_t} \left(\boldsymbol{Q}_1 - \nabla_h \cdot (\mathbf{E}\varphi) \right) + \boldsymbol{r}\left(\left[\!\!\left[\widehat{\mathbf{E}\varphi} \hat{n} - \mathbf{E}\varphi \hat{n} \right]\!\!\right] \right) + \boldsymbol{\ell}\left(\left\{\!\!\left\{ \widehat{\mathbf{E}\varphi} \hat{n} - \mathbf{E}\varphi \hat{n} \right\}\!\!\right\} \right)\,. \tag{25}$$

Inserting this result into the zeroth moment and using the definitions of $\boldsymbol{r}$ and $\boldsymbol{\ell}$:

$$\begin{aligned} \int_\Gamma [\![u]\!] \left\{\!\!\left\{ \widehat{\boldsymbol{J}} \cdot \hat{n} \right\}\!\!\right\} \mathrm{d}s + \int_{\Gamma_0} \{\!\{ u \}\!\} \left[\!\!\left[\widehat{\boldsymbol{J}} \cdot \hat{n} \right]\!\!\right] \mathrm{d}s + \int_\Gamma \left\{\!\!\left\{ \frac{\nabla_h u}{\sigma_t} \right\}\!\!\right\} \cdot \left[\!\!\left[\widehat{\mathbf{E}\varphi} \hat{n} - \mathbf{E}\varphi \hat{n} \right]\!\!\right] \mathrm{d}s \\ + \int_{\Gamma_0} \left[\!\!\left[\frac{\nabla_h u}{\sigma_t} \right]\!\!\right] \cdot \left\{\!\!\left\{ \widehat{\mathbf{E}\varphi} \hat{n} - \mathbf{E}\varphi \hat{n} \right\}\!\!\right\} \mathrm{d}s + \int \nabla_h u \cdot \frac{1}{\sigma_t} \nabla_h \cdot (\mathbf{E}\varphi) \,\mathrm{d}\mathbf{x} + \int \sigma_a \, u\varphi \,\mathrm{d}\mathbf{x} \\ = \int u \, Q_0 \,\mathrm{d}\mathbf{x} + \int \nabla_h u \cdot \frac{\boldsymbol{Q}_1}{\sigma_t} \,\mathrm{d}\mathbf{x}\,. \end{aligned} \tag{26}$$

Through the specification of the numerical fluxes, Eq. 26 defines a *family* of DG methods. An interior penalty-like choice of numerical fluxes is

$$\widehat{\boldsymbol{J}} \cdot \hat{n} = \left\{\!\!\left\{ \frac{1}{\sigma_t} \left(\boldsymbol{Q}_1 - \nabla_h \cdot (\mathbf{E}\varphi) \right) \cdot \hat{n} \right\}\!\!\right\} + \kappa \, [\![\varphi]\!]\,, \quad \widehat{\mathbf{E}\varphi} \hat{n} = \{\!\{ \mathbf{E}\varphi \hat{n} \}\!\}\,, \quad \text{on } \mathcal{F} \in \Gamma_0\,, \tag{27}$$

where κ is the penalty parameter. Boundary conditions are applied by setting

$$\widehat{\boldsymbol{J}} \cdot \hat{n} = 2\bar{J}_{\text{in}} + E_b \varphi \,, \quad \widehat{\mathbf{E}\varphi}\hat{n} = \mathbf{E}\varphi\hat{n} \,, \quad \text{on } \mathcal{F} \in \Gamma_b \,. \tag{28}$$

With these choices,

$$\left[\!\left[\widehat{\mathbf{E}\varphi}\hat{n} - \mathbf{E}\varphi\hat{n}\right]\!\right] = \begin{cases} -\left[\!\left[\mathbf{E}\varphi\hat{n}\right]\!\right] \,, & \mathcal{F} \in \Gamma_0 \\ 0 \,, & \mathcal{F} \in \Gamma_b \end{cases} \,, \quad \left\{\!\left\{\widehat{\mathbf{E}\varphi}\hat{n} - \mathbf{E}\varphi\hat{n}\right\}\!\right\} = 0 \,, \tag{29a}$$

$$\left\{\!\left\{\widehat{\boldsymbol{J}} \cdot \hat{n}\right\}\!\right\} = \widehat{\boldsymbol{J}} \cdot \hat{n} \,, \quad \left[\!\left[\widehat{\boldsymbol{J}} \cdot \hat{n}\right]\!\right] = 0 \,. \tag{29b}$$

Thus, the final form for an interior penalty-like DG discretization with Miften-Larsen boundary conditions is: find $\varphi \in Y_p$ such that

$$\begin{aligned} \int_{\Gamma_0} \kappa \, [\![u]\!] \, [\![\varphi]\!] \, \mathrm{d}s - \int_{\Gamma_0} [\![u]\!] \left\{\!\left\{ \frac{1}{\sigma_t} \nabla_h \cdot (\mathbf{E}\varphi) \cdot \hat{n} \right\}\!\right\} \mathrm{d}s - \int_{\Gamma_0} \left\{\!\left\{ \frac{\nabla_h u}{\sigma_t} \right\}\!\right\} \cdot [\![\mathbf{E}\varphi\hat{n}]\!] \, \mathrm{d}s + \int_{\Gamma_b} E_b \, u\varphi \, \mathrm{d}s \\ + \int \nabla_h u \cdot \frac{1}{\sigma_t} \nabla_h \cdot (\mathbf{E}\varphi) \, \mathrm{d}\mathbf{x} + \int \sigma_a \, u\varphi \, \mathrm{d}\mathbf{x} = \int u \, Q_0 \, \mathrm{d}\mathbf{x} + \int \nabla_h u \cdot \frac{\boldsymbol{Q}_1}{\sigma_t} \, \mathrm{d}\mathbf{x} \\ - 2 \int_{\Gamma_b} u \, \bar{J}_{\text{in}} \, \mathrm{d}s - \int_{\Gamma_0} [\![u]\!] \left\{\!\left\{ \frac{\boldsymbol{Q}_1 \cdot \hat{n}}{\sigma_t} \right\}\!\right\} \mathrm{d}s \end{aligned} \tag{30}$$

holds for all $u \in Y_p$. The penalty parameter is chosen as

$$\kappa = \left\{\!\left\{ \frac{(p+1)^2}{\sigma_t h} \right\}\!\right\} \tag{31}$$

where p is the polynomial order and h the mesh size. The inclusion of $1/\sigma_t$ in the penalty parameter ensures that over penalization does not occur in the thick diffusion limit.

4. SUBSPACE CORRECTION PRECONDITIONER

In [7], it is shown that the space Y_p can be decomposed into a direct sum of an $H^1(\mathcal{D})$ finite element space (i.e. continuous finite element space) and a DG space. Solvers known to be effective for continuous finite element discretizations of elliptic problems, such as Algebraic Multigrid (AMG), can then used on the continuous component of the solution and classical smoothers, such as Jacobi or Gauss-Seidel, can be applied on the DG component. This combination was shown to effectively precondition independently of the mesh size, polynomial order, and penalty parameter. The $H^1(\mathcal{D})$ operator corresponding to Eq. 30 is formed *algebraically* by assembling the DG system onto a continuous finite element space of the same polynomial order. In the results that follow, we use the stabilized bi-conjugate gradient method (BiCGStab) preconditioned by this subspace correction method. One AMG v-cycle and one Jacobi iteration are performed at each inner iteration.

5. RESULTS

The Method of Manufactured Solutions (MMS) is used to demonstrate the accuracy of the DG VEF method. The MMS solution is set to

$$\psi = \frac{1}{4\pi} \left[\sin(\pi x) \sin(\pi y) + \mu\eta \sin(2\pi x) \sin(2\pi y) + \mu^2 \sin\left(\frac{3\pi(x+\delta)}{1+2\delta} \right) \sin\left(\frac{3\pi(y+\delta)}{1+2\delta} \right) + \gamma \right] \tag{32}$$

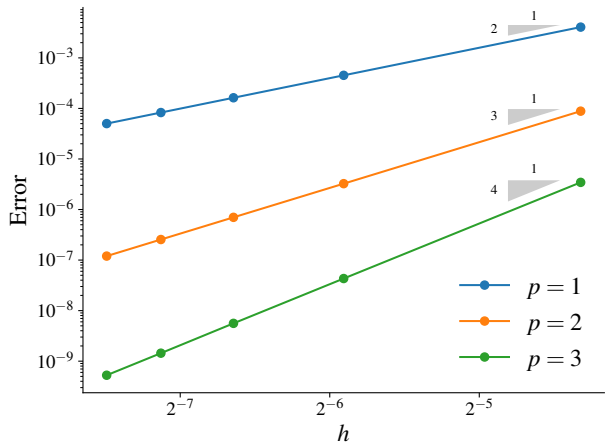

Figure 1: MMS error as a function of the mesh size, h, for the DG VEF MMS problem.

where $\boldsymbol{\Omega} = \begin{bmatrix}\mu & \eta\end{bmatrix}^T$. The parameters $\delta = 0.1$ and $\gamma = 0.5$ control the amount of spatially varying, quadratically anisotropic inflow and uniform, isotropic inflow, respectively. This form is chosen so that the Eddington tensor will be spatially varying and have non-zero off-diagonal components. Trigonometric functions are used so that the solution cannot be exactly represented by polynomials. The MMS scalar flux is then

$$\phi = \sin(\pi x)\sin(\pi y) + \frac{1}{3}\sin\left(\frac{3\pi(x+\delta)}{1+2\delta}\right)\sin\left(\frac{3\pi(y+\delta)}{1+2\delta}\right) + \gamma\,. \tag{33}$$

To test the use of multiple materials, the material data is set to

$$\sigma_t = \begin{cases} 10e^{-10\|\mathbf{x}-\mathbf{c}\|^2}\,, & \mathbf{x} \in [0.25, 0.75]^2 \\ 0.1\,, & \text{otherwise} \end{cases}\,, \quad \sigma_s = \sigma_t - 0.1\,, \tag{34}$$

with $\boldsymbol{c} = \begin{bmatrix}0.5 & 0.5\end{bmatrix}^T$ and $\mathcal{D} = [0,1]^2$. The mesh aligns with the jump in σ_t. These MMS angular and scalar flux solutions are substituted into the transport equation to solve for the MMS fixed-source, q. The accuracy of the DG VEF discretization can be ascertained independent from transport by projecting the MMS angular flux onto a discrete angular flux in the space Y_p that is then used to compute the VEF data. The MMS source q is integrated with angular quadrature to form the source moments Q_0 and $\boldsymbol{Q}_1$. The computation of the VEF data is performed with S_4 angular quadrature. A finite element space with open node placement on each element is used so that the projection yields a discrete angular flux grid function, and thus an Eddington tensor, that has discontinuities of magnitude $\mathcal{O}(h^{p+1})$ on interior faces. The VEF equations are then solved as if $\mathbf{E}$, E_b, Q_0, and $\boldsymbol{Q}_1$ are given data. Figure 1 shows the error in the $L^2(\mathcal{D})$ norm as a function of the mesh size for three polynomial orders. All values of p converge as $\mathcal{O}(h^{p+1})$ as expected.

Next, we verify the DG VEF method maintains the thick diffusion limit. The problem parameters are:

$$\sigma_t = \frac{1}{\varepsilon}\,, \quad \sigma_s = \frac{1}{\varepsilon} - \varepsilon\,, \quad q = \varepsilon\,, \quad \mathcal{D} = [0,1]^2\,, \tag{35}$$

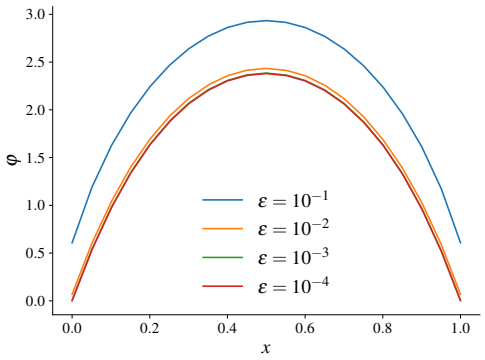

Figure 2: Lineouts of the 2D thick diffusion limit problem as $\varepsilon \to 0$.

and vacuum boundary conditions. S_4 angular quadrature was used. Figure 2 shows lineouts of the VEF scalar flux solution along the y-axis centerline for four values of ε. A coarse mesh of 16×16 elements was used and $p = 2$. These solutions are not the trivial zero solution and thus this DG VEF method has the thick diffusion limit. Here, the full coupled transport-VEF system is solved using fixed-point iteration. Fixed-point iteration converged to a tolerance of 10^{-8} in 11, 8, 5, and 4 iterations for $\varepsilon = \{10^{-1}, 10^{-2}, 10^{-3}, 10^{-4}\}$.

Finally, the full DG VEF transport iteration is tested on the linearized crooked pipe problem. The geometry is shown in Fig. 3a. The "pipe" region is in gold and the "wall" region is in blue. The material data corresponding to the pipe and wall are given in Table 1. Isotropic inflow of magnitude $\frac{1}{2\pi}\mathrm{cm}^{-2}\,\mathrm{sr}^{-1}$ impinges on the left opening of the pipe. The rest of the boundary is treated as vacuum. The source corresponds to the first time step of a linearized thermal radiative transfer calculation with $c\Delta t = 1000\,\mathrm{m}$ and initial angular flux of $10^{-4}\mathrm{cm}^{-2}\,\mathrm{sr}^{-1}$. This problem has a discontinuous inflow function and a 1000x difference in total cross section making it a difficult problem to test the DG VEF algorithm. One of the computed solutions is shown in Fig. 3b. S_{10} angular quadrature was used. The outer tolerance was 10^{-6} and the inner BiCGStab tolerance was 10^{-7}. The quadratic programming-based negative flux fixup from [6] was used to fixup the angular flux at each outer iteration. Figure 4 shows the number of inner BiCGStab iterations required for convergence at each outer iteration when BiCGStab is passed the previous outer iteration's solution as an initial guess and when a zero initial guess is used. A 32×32 mesh was used with $p = 2$. Using the outer iteration as an initial guess significantly reduced the total number of inner iterations required in the calculation from 542 to 342.

Table 2 shows the number of outer and inner iterations needed for three polynomial orders and three mesh refinements for the linearized crooked pipe problem. The previous outer iteration's solution is used as the initial guess for the inner iteration. The number of outer iterations is consistent with that of the VEF method from [5]. The outer iteration does increase with p: this is likely due to the increased need for the negative flux fixup with larger p. The primary result of this paper is the efficiency of the inner iteration: preconditioned BiCGStab converges uniformly for all the mesh sizes and polynomial orders tested.

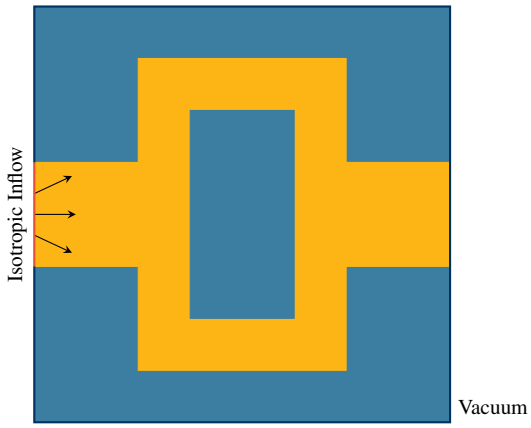

(a) Geometry and materials for the linearized crooked pipe problem.

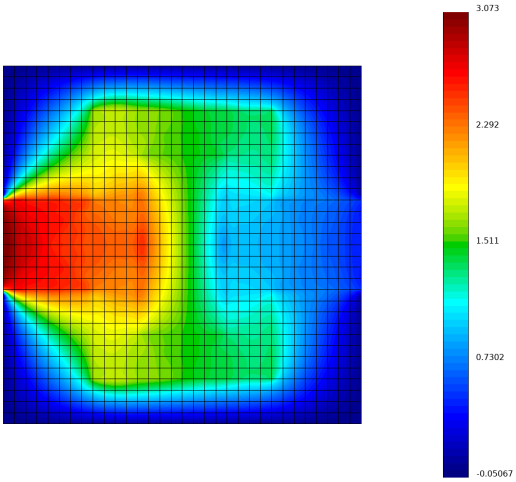

(b) Scalar flux solution with $p = 3$ on a mesh of 32×32 elements.

Table 1: Material data for the linearized crooked pipe problem.

	Pipe	Wall
σ_t	$0.2\,\mathrm{cm}^{-1}$	$200\,\mathrm{cm}^{-1}$
σ_a	$0.001\,\mathrm{cm}^{-1}$	$0.001\,\mathrm{cm}^{-1}$
q	$0.1\,\mathrm{cm}^{-3}\,\mathrm{sr}^{-1}$	$0.1\,\mathrm{cm}^{-3}\,\mathrm{sr}^{-1}$

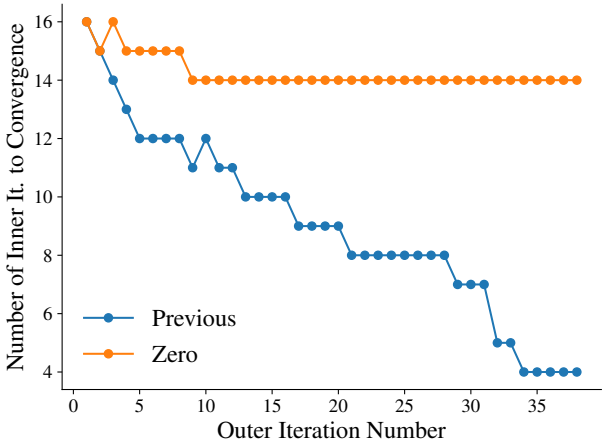

Figure 4: Number of inner BiCGStab iterations at each outer iteration when the previous outer iteration is used as the initial guess compared to using a zero initial guess.

Table 2: Number of outer and inner iterations until convergence on the linearized crooked pipe problem.

	N_e	Outer It.	Total Inner It.	Min Inner It.	Max Inner It.	Avg. Inner It.
$p=1$	256	23	200	3	15	8.7
	1024	30	277	3	17	9.23
	4096	36	336	3	17	9.33
$p=2$	256	31	285	3	16	9.19
	1024	38	342	4	16	9.0
	4096	48	442	4	15	9.21
$p=3$	256	35	390	3	19	11.14
	1024	45	515	4	20	11.44
	4096	56	653	5	20	11.66

REFERENCES

[1] D. Mihalas. *Stellar Atmospheres*. W. H. Freeman and Co (1978).

[2] V. Ya. Gol'din. "A Quasi-Diffusion Method of Solving the Kinetic Equation." *USSR Comp Math and Math Physics*, **volume 4**, pp. 136–149 (1964).

[3] J. Warsa and D. Anistratov. "Two-Level Transport Methods with Independent Discretization." *Journal of Computational and Theoretical Transport*, **volume 47**(4-6), pp. 424–450 (2018).

[4] S. S. Olivier and J. E. Morel. "Variable Eddington Factor Method for the SN Equations with Lumped Discontinuous Galerkin Spatial Discretization Coupled to a Drift-Diffusion Acceleration Equation with Mixed Finite-Element Discretization." *Journal of Computational and Theoretical Transport*, **volume 46**(6-7), pp. 480–496 (2017).

[5] S. Olivier, P. Maginot, and T. Haut. "High Order Mixed Finite Element Discretization for the Variable Eddington Factor Equations." In *Proceedings of the International Conference on Mathematics and Computational Methods Applied to Nuclear Science and Engineering (M&C 2019)* (2019).

[6] B. C. Yee, S. S. Olivier, T. S. Haut, M. Holec, V. Z. Tomov, and P. G. Maginot. "A quadratic programming flux correction method for high-order DG discretizations of SN transport." *Journal of Computational Physics*, **volume 419**, p. 109696 (2020).

[7] W. Pazner and T. Kolev. "Uniform subspace correction preconditioners for discontinuous Galerkin methods with hp-refinement." *ArXiv*, **volume abs/2009.01287** (2020).

[8] D. N. Arnold, F. Brezzi, B. Cockburn, and L. D. Marini. "Unified Analysis of Discontinuous Galerkin Methods for Elliptic Problems." *SIAM Journal on Numerical Analysis*, **volume 39**(5), pp. 1749–1779 (2002).

[9] T. S. Haut, P. G. Maginot, V. Z. Tomov, B. S. Southworth, T. A. Brunner, and T. S. Bailey. "An Efficient Sweep-Based Solver for the SN Equations on High-Order Meshes." *Nuclear Science and Engineering* (2019).